



**UNIVERSITY OF LEEDS**

This is a repository copy of *Performance of rapid hardening recycled clean steel fibre materials*.

White Rose Research Online URL for this paper:  
<http://eprints.whiterose.ac.uk/138911/>

Version: Accepted Version

---

**Article:**

Al-musawi, H, Figueiredo, FP, Bernal, SA [orcid.org/0000-0002-9647-3106](https://orcid.org/0000-0002-9647-3106) et al. (2 more authors) (2019) Performance of rapid hardening recycled clean steel fibre materials. *Construction and Building Materials* (195). pp. 483-496. ISSN 0950-0618

<https://doi.org/10.1016/j.conbuildmat.2018.11.026>

---

© 2018 Elsevier Ltd. Licensed under the Creative Commons Attribution-NonCommercial-NoDerivatives 4.0 International License (<http://creativecommons.org/licenses/by-nc-nd/4.0/>).

**Reuse**

This article is distributed under the terms of the Creative Commons Attribution-NonCommercial-NoDerivatives (CC BY-NC-ND) licence. This licence only allows you to download this work and share it with others as long as you credit the authors, but you can't change the article in any way or use it commercially. More information and the full terms of the licence here: <https://creativecommons.org/licenses/>

**Takedown**

If you consider content in White Rose Research Online to be in breach of UK law, please notify us by emailing [eprints@whiterose.ac.uk](mailto:eprints@whiterose.ac.uk) including the URL of the record and the reason for the withdrawal request.



[eprints@whiterose.ac.uk](mailto:eprints@whiterose.ac.uk)  
<https://eprints.whiterose.ac.uk/>

# 1 Performance of rapid hardening recycled clean steel fibre materials

2 Hajir Al-musawi <sup>a,\*</sup>, Fabio P. Figueiredo <sup>a</sup>, Susan A. Bernal <sup>b</sup>, Maurizio Guadagnini <sup>a</sup>, Kypros

3 Pilakoutas <sup>a</sup>

4 <sup>a</sup>Department of Civil and Structural Engineering, The University of Sheffield, Sir Frederick Mappin Building, Mappin  
5 Street, S1 3JD Sheffield, UK.

6 <sup>b</sup> School of Civil Engineering, University of Leeds, Woodhouse Lane, Leeds, LS2 9JT, United Kingdom.

7 \* Corresponding author's email: [Haal-musawi1@sheffield.ac.uk](mailto:Haal-musawi1@sheffield.ac.uk) Tel: +44 (0) 114 222 5729, Fax: +44 (0) 114 2225700

## 8 HIGHLIGHTS

- 9 • Mixes achieve 90% of their one year flexural strength at the age of one day.
- 10 • RCSF enhances flexural strength and toughness resulting in hardening behaviour.
- 11 • Constitutive equations based on the RILEM and MC 2010 recommendations overestimate loading  
12 capacity.
- 13 • FEA analysis using multilinear  $\sigma - \epsilon$  tensile curves obtained by inverse analysis can capture well the  
14 post cracking strength and cracking pattern.

## 15 Abstract

16 To minimise disruption due to repairs of concrete pavements, rapid hardening and tough materials need  
17 to be used. This paper investigates the flexural performance of rapid hardening mortar mixes made with  
18 two commercial cement types, calcium sulfo-aluminate cement and calcium aluminate cement, for thin  
19 concrete repair applications. Three-point bending tests are performed on plain and steel fibre reinforced  
20 concrete specimens containing 45 kg/m<sup>3</sup> of recycled clean steel fibres to characterise the flexural

21 performance of notched and unnotched prisms at different ages, ranging from one hour up to one year.  
22 The recycled fibers are shown to enhance both the flexural strength and toughness of FRC prisms, leading  
23 to hardening behaviour. Constitutive equations based on the RILEM and Model Code 2010  
24 recommendations are found to overestimate the loading capacity of the bending tests. FE analyses using  
25 multilinear  $\sigma - \epsilon$  tensile curves obtained by employing inverse analysis can capture better the post cracking  
26 strength and cracking pattern of the tested prisms.

27 **Key words:** SFRC, recycled clean steel fibres, rapid hardening cements, mechanical properties, FEA

## 28 **1. Introduction**

29 Progressive deterioration of infrastructure, particularly pavements, occurs due to increasing vehicular axle  
30 loads, worsening environmental conditions (due to climate change) and higher traffic volumes. Excessive  
31 deterioration can lead to serious service disruptions and higher costs for infrastructure owners and road  
32 users. Conventional ordinary Portland cement (OPC) based repair materials attain their strength rather  
33 slowly and need between 12h to 24h to develop sufficient strength before roads can be back in service,  
34 adding to delays and disruption during maintenance. To minimise disruption, rapid hardening cements  
35 can be used in repairs. There are several special rapid hardening Portland-free cements available in the  
36 market; such as calcium sulfo-aluminate (CSA) cement and calcium aluminate (CA) cement. CSA can  
37 achieve early rapid strength development even in cold environments and can have expansive properties.  
38 It is reported to have good durability in aggressive environments, particularly when exposed to sulfates  
39 [2]. Furthermore, this cement requires less energy for its production compared to OPC [1], thus it is  
40 considered to be environmentally friendly. However, despite its lower energy demand, it is still more  
41 expensive due to the cost of its raw materials.

42 CA cements are characterised by high early strength development and high resistance to elevated  
43 temperatures, depending on their aluminum content. An important aspect for the rapid strength

44 development of this cement is the substantial amount of heat of hydration which can result in high heat  
45 generation [3]. Self-heating may be a concern in sections thicker than 100 mm [3], but not necessarily for  
46 thinner repair layers. Despite the high temperature rise during hydration, CA concretes do not seem to be  
47 overly susceptible to thermal cracking. This may be due to creep relaxation of thermally induced strains,  
48 facilitated by a conversion reaction, during which some metastable phases of this cement convert to  
49 stable phases of lower volume [3, 4]. As porosity increases, the densification due to conversion causes  
50 loss of strength [3]. Hence, when used for repairs, the key concern to be addressed is cracking due to  
51 restrained shrinkage.

52 Restrained shrinkage is one of the main factors that govern the serviceability and durability of concrete  
53 repairs [5,6]. Shrinkage in concrete results due to moisture diffusion from the new concrete to the  
54 environment and to the concrete substrate [7] if not adequately saturated. However, shrinkage  
55 deformation (of the new layer) is restrained by the substrate layer leading to the development of tensile  
56 and interfacial shear stresses. If these stresses exceed the material capacity at any time, cracking will  
57 develop in the repair material and/or debonding along the interface between the repair material and the  
58 substrate. Micro-cracks induced by shrinkage can propagate and coalesce into macro-cracks under the  
59 effect of applied loads.

60 Cracks beyond a certain width can adversely affect the durability of repair materials by creating easy  
61 access for deleterious agents leading to early saturation, freeze–thaw damage, scaling, and steel  
62 corrosion, which promote further internal and external cracking and accelerate the rate of deterioration  
63 [8]. This issue can be worsen with rapid hardening (non-expansive) materials due to the rapid hydration  
64 rate which accelerates shrinkage development. Furthermore, due to the rapid stiffness development and  
65 decrease in creep compliance of rapid hardening cements [9], their ability to redistribute stresses may be  
66 affected, thereby increasing cracking potential. To address this issue, fibres can be added to control crack  
67 widths [10] as well as increase the tensile strength and fatigue resistance [11], thus resulting in more

68 durable layers. To reduce the environmental impact of manufactured steel fibres (MSF), recycled clean  
69 steel fibres (RCSF) can be used as alternative fibre reinforcement.

70 During the manufacture of tyres, parallel steel cords are embedded in continuous thin rubber belts. After  
71 being cut to shape, these are placed in overlapping layers to provide flexible reinforcement within the  
72 tread and side walls of the tyre. The complex configuration of each layer generates significant levels of  
73 waste (approximately 5% by mass). The available amount of waste steel cord is therefore around 100,000  
74 tonnes per year worldwide. The steel reinforcement used in tyre manufacture typically consists of parallel  
75 filaments of very fine wire (0.1-0.4 mm dia.) twisted together to form a cord about 0.5-1.0 mm in diameter  
76 [12]. Recycled clean steel fibre (RCSF) filaments extracted from pre-vulcanised rubber belt offcuts have  
77 become available recently and were adopted in this study. However, knowledge on their use in concrete  
78 is scarce and it is limited to research at the University of Sheffield [13]. Knowledge of the effect of  
79 industrial fibres on CSA and CA matrices is also rather limited [9,14-16] and no published data exist  
80 regarding the effect of RCSF. A study on the effect of CSA matrix on pullout performance of steel fibres  
81 [9] suggests that the synergetic effect of a stiff matrix like ettringite and high modulus steel fibres can  
82 increase crack propagation in the composite material, evidenced by an increase in debonding energy  
83 density.

84 Since cracking is the main concern for repairs, understanding the effect of fibres in controlling crack widths  
85 under mechanical and hygral loads, as well as the complex interaction of shrinkage, stiffness and tensile  
86 strength evolution are of paramount importance. For this purpose, finite element analysis can be a useful  
87 tool. However, appropriate material parameters need to be determined experimentally and the tensile  $\sigma$ -  
88  $\epsilon$  curves of the repair materials need to be derived from direct tension or bending results. Although there  
89 are several procedures in the literature to derive the  $\sigma$ - $\epsilon$  of SFRC in tension [17-20], they may not be  
90 entirely suitable for modelling mortars reinforced with RCSF due to the different fracture energies of the  
91 two concretes. In numerical studies performed by [20, 21], it was found that RILEM proposed  $\sigma$ - $\epsilon$

92 equations overestimate the predicted capacity of FRC. As a result, a simplified  $\sigma$ - $\epsilon$  model was suggested  
93 to overcome issues in the other methods and to include the post-consumer tyres steel fibres (RTSF) effect.  
94 This paper presents experimental and numerical work on the flexural performance of RCSF on rapid  
95 hardening mortars produced using CSA or CA as sole cementitious materials. Constitutive relationships  
96 derived based on code recommendations and by others [19, 20] are used to predict flexural behaviour  
97 and the results are compared with predictions obtained from inverse analysis.

## 98 **2. Experimental details and methodology**

### 99 **2.1. Materials**

100 Two commercial cement types were used in this study; calcium sulfoaluminate cement<sup>1</sup> (CSA) and rapid  
101 setting calcium aluminate cement<sup>2</sup> (RSC). According to the manufacturer, RSC consists of hydrated  
102 alumina, oxides of iron and titanium, with small amounts of silica. For production of mortars, fine  
103 aggregates, medium grade river washed sand (0-5mm sourced from Shardlow in Derbyshire, UK, SG=2.65,  
104 A = 0.5, FM = 2.64), were used. Recycled clean steel fibres (RCSF) were obtained from tyre cords extracted  
105 from un-vulcanised rubber belts (see Figure 1). The length of the RCSF used in this study was 21 mm and  
106 the diameter 0.2 mm. The strength of these fibres is reported to exceed 2600 MPa [13]. Superplasticiser<sup>3</sup>  
107 was added to enhance the workability and adjust the setting time.

108



109

110

**Figure 1.** Photograph of the RCSF used in this study

111 **2.2. Mortar mix design**

112 A total of 600 kg/m<sup>3</sup> of cement was used with low w/c ratios to obtain high early strength. For durability  
113 requirements, w/c should be kept lower than 0.4. However, as CSA cement consumes more water to form  
114 hydration products than ordinary Portland cement [22], this limit can be relaxed slightly for this cement.  
115 As a result, two different w/c ratios and SP dosages were tested. The w/c ratios for mixes with CSA cement  
116 were 0.4 and 0.41, and 0.35 and 0.36 for RSC mixes. The water content and superplasticiser (SP) were  
117 carefully selected to achieve a workable mix with setting time of no longer than 15 minutes. Fibre dosage  
118 of 45 kg/m<sup>3</sup> ( $V_f = 0.57\%$ ) was investigated as is commonly used in European practice for structural  
119 applications. The plain and fibre reinforced mortar mixes for each cement type are almost identical, to  
120 reliably investigate the effect of fibres on the mechanical properties. The details of the optimised mortar  
121 mixes are summarised in Table 1.

122 The specimens were cured for one hour before demoulding and exposure to standard laboratory  
123 conditions.

124 **Table 1**

125 Mortar mix composition

mix	Cement (kg/m <sup>3</sup> )	w/c	Sand (kg/m <sup>3</sup> )	SP <sup>a</sup>	Fibre dosage (kg/m <sup>3</sup> )
CSA	600	0.40	1420	0.60	0
FCSA	600	0.41	1420	0.61	45
RSC <sup>b</sup>	600	0.35	1300	0.20	0
FRSC	600	0.36	1300	0.21	45

126 <sup>a</sup> % by cement mass. <sup>b</sup> mixes containing CA cement are called RSC in this study.

127

128 **2.3. Fresh state properties**

---

<sup>1</sup> provided by Kershin International Co., Ltd

<sup>2</sup> sourced from Instarmac

<sup>3</sup> Sika Viscoflow 2000

129 **2.3.1. Vicat test**

130 The setting time of cement pastes was assessed using an automatic Vicat apparatus according to ASTM  
131 C191 (2013) [23]. As the cements used in this study are fast setting, the instrument was set to take  
132 measurements every 30 seconds.

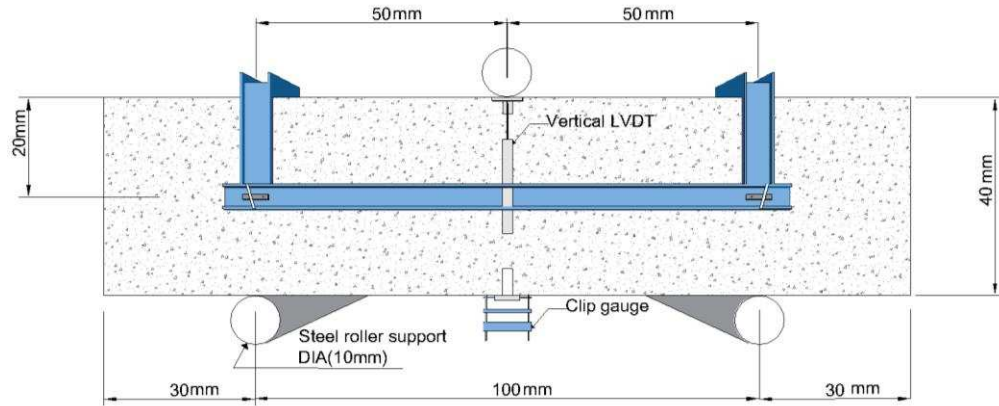
133 **2.3.2. Semi-adiabatic calorimetry**

134 The semi-adiabatic calorimeter records the temperature evolution and key temperature related  
135 properties for a tested mix, such as time to peak heat, peak heat, and cumulative heat [24]. Since the  
136 mortar mixes are designed for thin repairs, heat loss due to dissipation is expected to take place and  
137 hence, the semi-adiabatic test could reveal a temperature evolution that is close to practical applications.  
138 After mixing the required quantity for each mix, the mortar was directly placed in an insulated thermal  
139 flask cylinder of 0.5 l and a thermocouple was inserted inside the mortar to record the temperature.

140 **2.4. Flexural tests**

141 To characterise the flexural performance, mortar prisms of 40 × 40 × 160 mm were tested according to BS  
142 EN 13892-2 [25]. To obtain the load deflection curve after the peak load, displacement control was  
143 adopted rather than load control as required by the standard. The rate of loading was 0.25 mm/min until  
144 1 mm deflection, and 1 mm/min after that. To eliminate errors due to machine stiffness, spurious support  
145 displacements and local concrete crushing, a specially designed aluminum yoke (based on the Japanese  
146 standard JSCE-SF4 [26]) was mounted on the specimens. To assess the flexural behaviour over time, the  
147 prisms were tested at one hour, three hours, one day, seven days, 28 days and 365 days. The test was also  
148 performed on notched prisms (the notch depths range from 3.57 to 4.94 mm) to assess crack  
149 development. The Crack Mouth Opening Displacement (CMOD) was measured at mid span with a 12.5  
150 mm clip gauge (mounted across the bottom part of the notch, Figure 2). For practical reasons, this test  
151 was performed at 2 days (at the earliest age) and up to one year.





152

153

**Figure 2.** Flexural test set up

154 **2.5. Compressive strength**

155 Directly after flexural testing, the halves of the fractured prisms were tested in uniaxial compression  
 156 according to BS EN 13892-2 [25]. Only the one-hour compressive strength of FRC specimens was examined  
 157 separately due to practical time constrains.

158 **3. Experimental Results and Discussion**

159 **3.1. Fresh state properties of rapid hardening materials**

160 The water content and SP dosage were optimised for each mix to achieve a workable mix with setting  
 161 time of no longer than 15 minutes. As shown in Table 2, the CSA cement had a relatively shorter setting  
 162 time compared to the RSC cement. Slightly higher water content and SP dosages for the fibre reinforced  
 163 mixes lead to a slight increase of the setting time for these mixes.

164 **Table 2**

165 Setting time and maximum temperature ( $T_{peak}$ ) for different mixes

Mixes	Vicat setting time (min.)		$T_{peak}$ ( $^{\circ}C$ )
	Initial	Final	
CSA	9.5	10.5	68
FCSA	9.5	11.0	68
RSC	12.0	14.5	91
FRSC	12.5	15.0	88

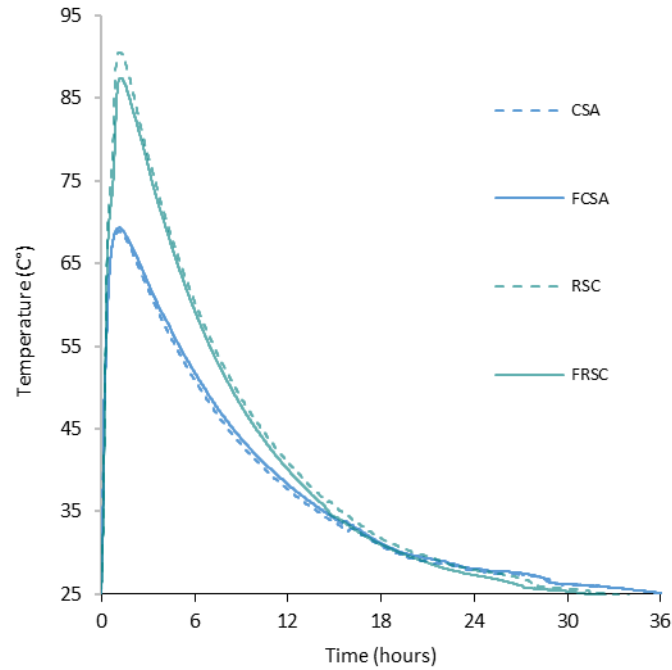
166

167 The results of the semi-adiabatic calorimetry test (for the first 36 hours) are shown in Figure 3. For mixes  
168 with CSA cement, the peak temperature ( $T_{\text{peak}}$ ) was about 68° C (see Table 2) occurring during the first  
169 hour regardless of fibre content. The temperature rise in RSC mixes was much higher than in mixes with  
170 CSA cement, with  $T_{\text{peak}}$  at 91° and 88° C for RSC and FRSC, respectively. The time half way to the peak ( $T_{1/2}$   
171  $_{\text{peak}}$ ) can be taken as an indication of the initial setting time of cementitious mixes [27]. For CSA and FCSA,  
172  $T_{1/2 \text{ peak}}$  was achieved at around 11 minutes, whilst for RSC and FRSC, it was recorded at around 16 minutes.  
173 These results agree well with the results of the vicat test. The temperature achieved for these cements  
174 upon hydration dropped to laboratory temperature in less than 24 hours. Heat dissipation is expected to  
175 occur faster onsite than in the semi-adiabatic test and, therefore, no major thermal cracking is expected  
176 for thin repairs, especially when curing is applied during the first two hours when  $T_{\text{peak}}$  occurs.

### 177 **3.2. Mechanical performance of rapid hardening mortars**

#### 178 **3.2.1. Compressive strength**

179 The average compressive strength  $f_{cu}$  (from six specimens) and standard deviation developed over time  
180 is shown in Figure 4. At one hour, FCSA achieved the highest compressive strength of 26.1 MPa while RSC  
181 achieved 17.2 MPa. This behavior changes at later ages as RSC achieves a higher strength than FCSA by  
182 approximately 6% after one-year. The fibres seem to have a positive effect on the compressive strength  
183 of both mortars, with the highest strength increase noticed at one hour (24% increase in  $f_{cu}$ ). At later ages,  
184 this increase ranges from 10% to 17%.



185

186

**Figure 3.** Temperature rise for mixes in semi-adiabatic test

187

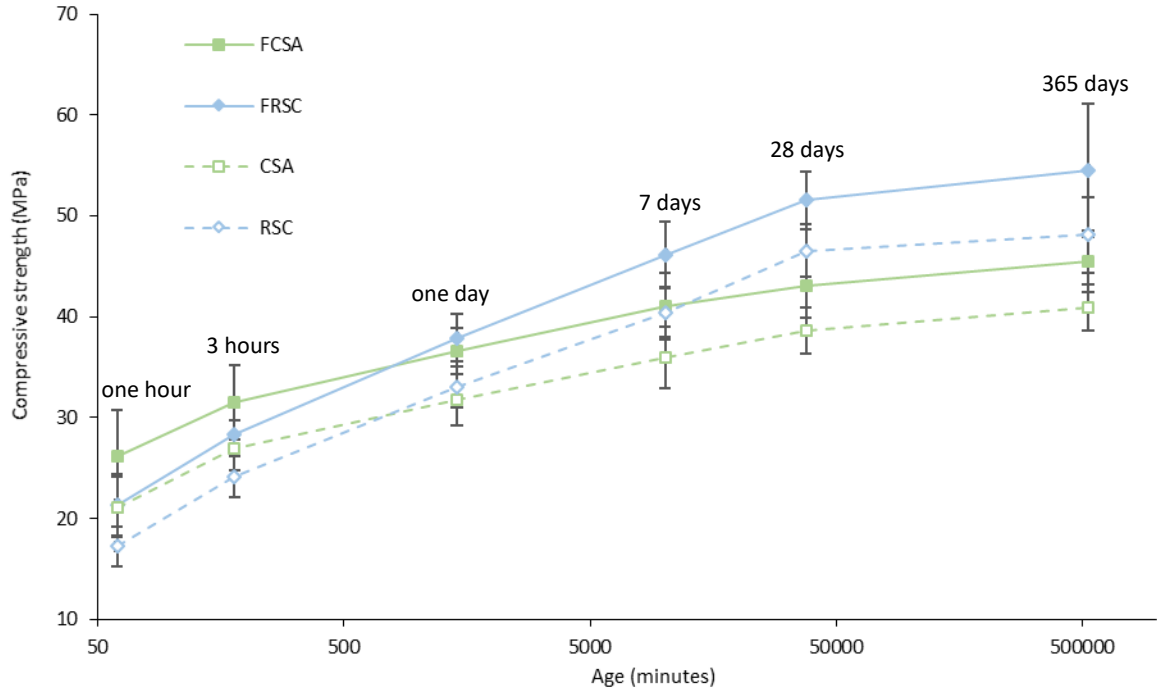
There is no consensus in literature on the effect of fibers on compressive strength. While some researchers [28-30] report a strength enhancement of up to 20% for Portland cement-based specimens containing recycled fibres with dosages less than 50 kg/m<sup>3</sup>, others [31-33] found only a marginal effect due to air entrainment.

189

191

No strength reduction has been observed for any of the mixes at the age of one-year, indicating that there were no significant conversion issues. It should be noted that for fully cured rapid hardening CSA mortar-based samples (tested at 28 days), a compressive strength of 31.4 – 52.6 MPa for w/c ratios 0.4 – 0.5 was reported in literature [34] and this agrees well with the results of this study.

194



195

196

**Figure 4.** Development of  $f_{cu}$  as a function of time

197

To describe the compressive strength development with time, the  $\beta_{cc}(t)$  function that describes the strength development with time used in Model Code 2010 [18] is followed.

198

$$\beta_{cc} = \exp\left\{s \cdot \left[1 - \left(\frac{28}{t}\right)^{0.5}\right]\right\} \quad \text{equation 1}$$

199

200

where,  $t$  is the concrete age in days,  $s$  is a coefficient that depends on the class of cement which ranges

201

from 0.2 – 0.38 for  $f_{cm} \leq 60$  MPa. As the cements used in this study are rapid hardening, a 0.2 value for  $s$

202

was adopted. To obtain the strength at various ages,  $\beta_{cc}(t)$  is multiplied by the mean compressive strength

203

at the age of 28 days ( $f_{cm}$ ). The estimated compressive strength at various ages is shown against the

204

experimental results in Figure 5. As expected, the function underestimates the strength at the early ages

205

by approximately 100% for the different rapid hardening mixes. As the strength evolves very rapidly at

206

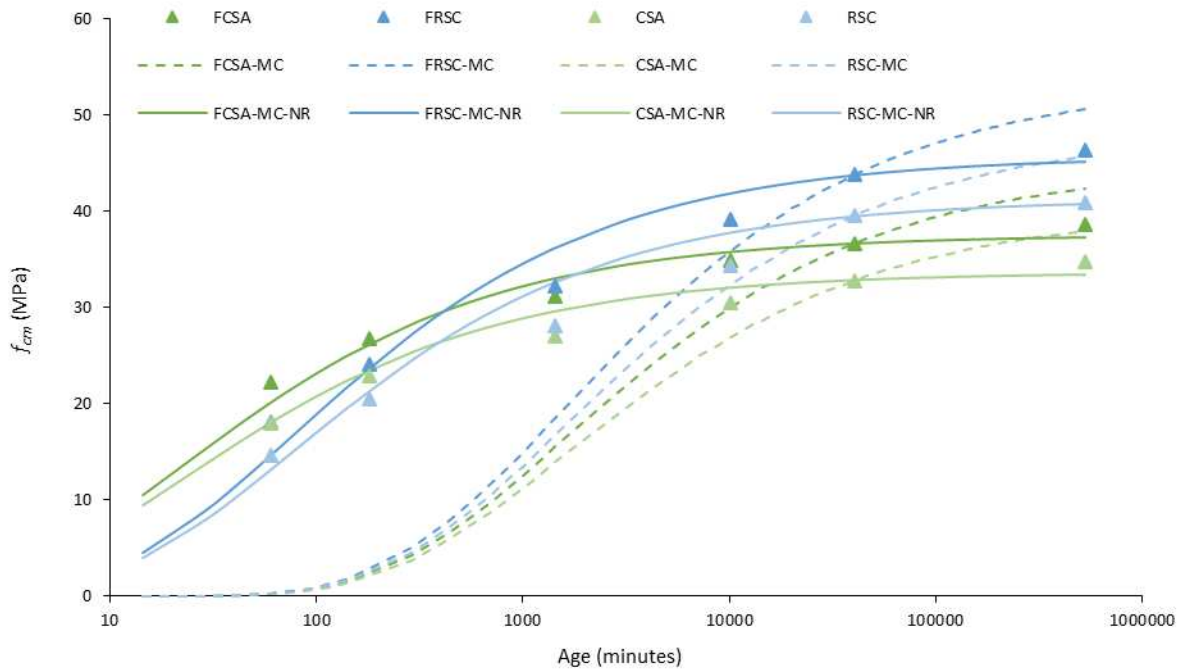
the early ages and then it slows down, smaller  $s$  values could offer a better representation for strength

207

development with time. The  $s$  values of 0.024 and 0.044 for mixes with CSA and RSC cements, respectively,

208

were found by regression analysis to represent well the strength evolution with time (see Figure 5).



209

210 **Figure 5.** Development of experimental and estimated  $f_{cm}$  as a function of time using  $s = 0.2$  (dashed lines) and  
 211 suggested  $s$  values (solid lines-NR)

212 **3.2.2. Flexural behaviour**

213 The average flexural strength development over time (and standard deviation) is illustrated in Figure 6.

214 The reported values represent the limit of proportionality (LOP), or first cracking strength ( $f_{ctm,fl}$ ),

215 determined according to BS EN 14651:2005 [35]. It is noted that strength develops very fast and both

216 plain and fibre reinforced specimens achieved 90% of their one-year strength in one day. The specimens

217 made with CSA cement showed higher flexural strength than those with CA cement tested at the same

218 age, probably due to the rigid dense crystal microstructure of the CSA cement [9]. RSC mixes have lower

219 w/c ratio, hence, their compressive strength is expected to be higher in the long term. Due to high

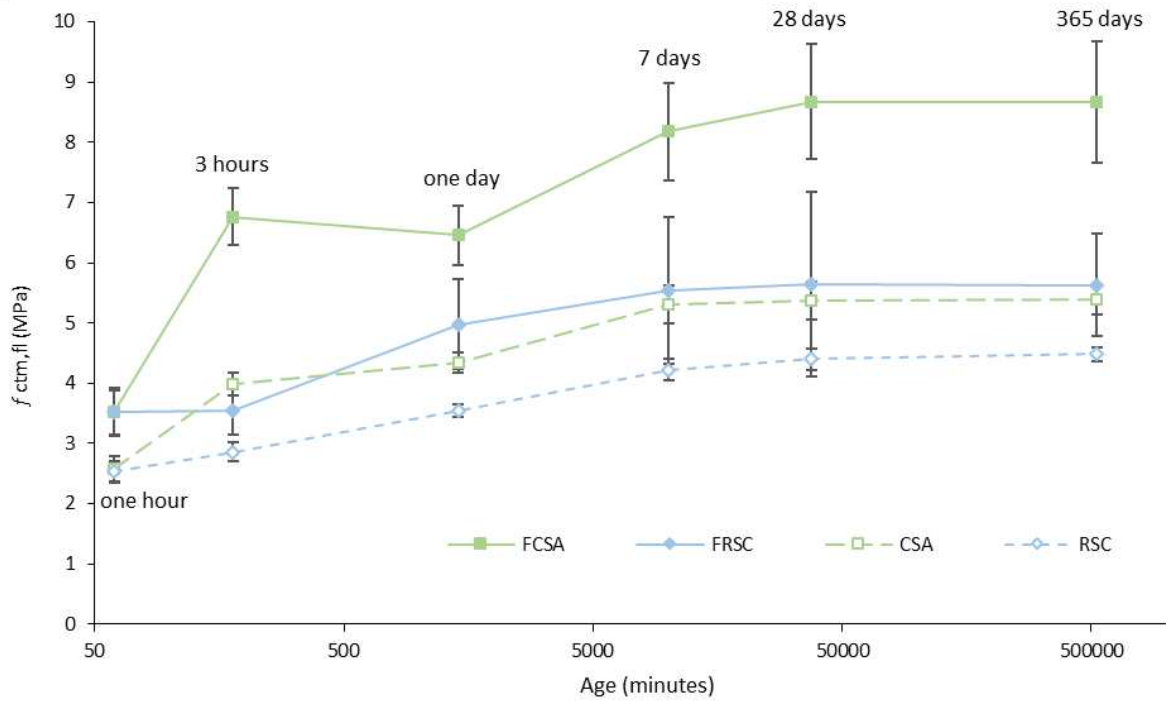
220 shrinkage in RSC mixes, their flexural strength is reduced. The effect of RCSF on the flexural strength

221 enhancement of the mixes is evident at all ages. Compared to their plain counterparts, FCSA and FRSC

222 mixes showed a flexural strength increase of approximately 36% to 70% and 24% to 41%, respectively.

223 This agrees well with Hu et al. [33], who reported an increase of 45% - 70% in  $f_{ctm,fl}$  of concrete reinforced

224 with blends of manufactured and post-consumer recycled fibres.



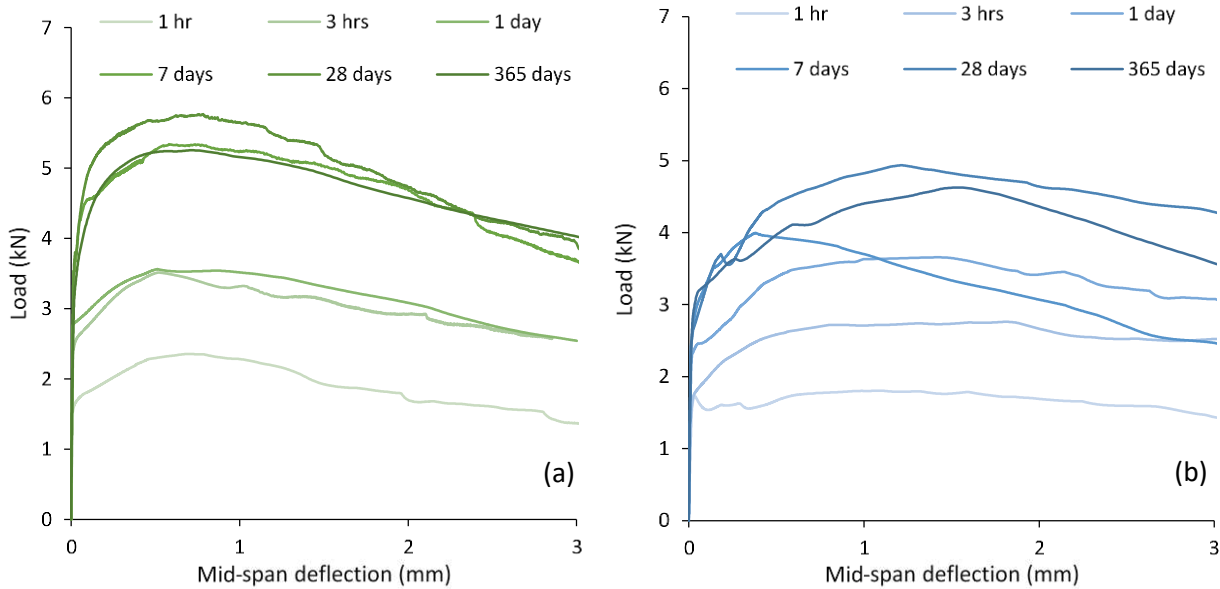
225

226 **Figure 6.** The flexural strength  $f_{ctm,fl}$  development as a function of time

227 The load-deflection curves for FCSA and FRSC prisms are shown in Figure 7. The behaviour of the  
228 specimens made with the unreinforced mixes is not shown as they failed suddenly after peak load without  
229 any post cracking strength, highlighting the poor toughness of plain mortars in tension. The deflection  
230 hardening shown by reinforced mixes can be attributed to the high number of fibres spanning the cracked  
231 section and the excellent bond between steel fibres and dense matrix systems, like the CSA cement. This  
232 hypothesis is supported by the fact that in the current study, many specimens developed more than one  
233 principal crack, confirming the excellent load transfer by the RCSF. It should be noted that the preferential  
234 alignment of the fibres in the direction of stress due to the small mould size ( $40 \times 40 \times 160$  mm) may have  
235 contributed to this. Deflection hardening was also reported in a study by Bordelon [36] for concrete  
236 specimens cut from prisms of  $150 \times 150 \times 450$  mm and tested using a 50 mm beam depth (to simulate a  
237 thin overlay). Deflection hardening performance for notched concrete prisms reinforced with  $45\text{kg/m}^3$  of

238 blends of recycled post-consumer and manufactured steel fibres was also reported in a recent study  
239 published by Hu et al. [33].

240 At large deflections (greater than 2 mm), the FCSA specimens show a slight reduction in load resistance  
241 compared to FRSC specimens, possibly due to the inherent brittleness of the CSA cement. However, in  
242 most repair applications, it is not expected that the mortar will reach such high level of deformation and  
243 as a result, minimal cracking is expected.

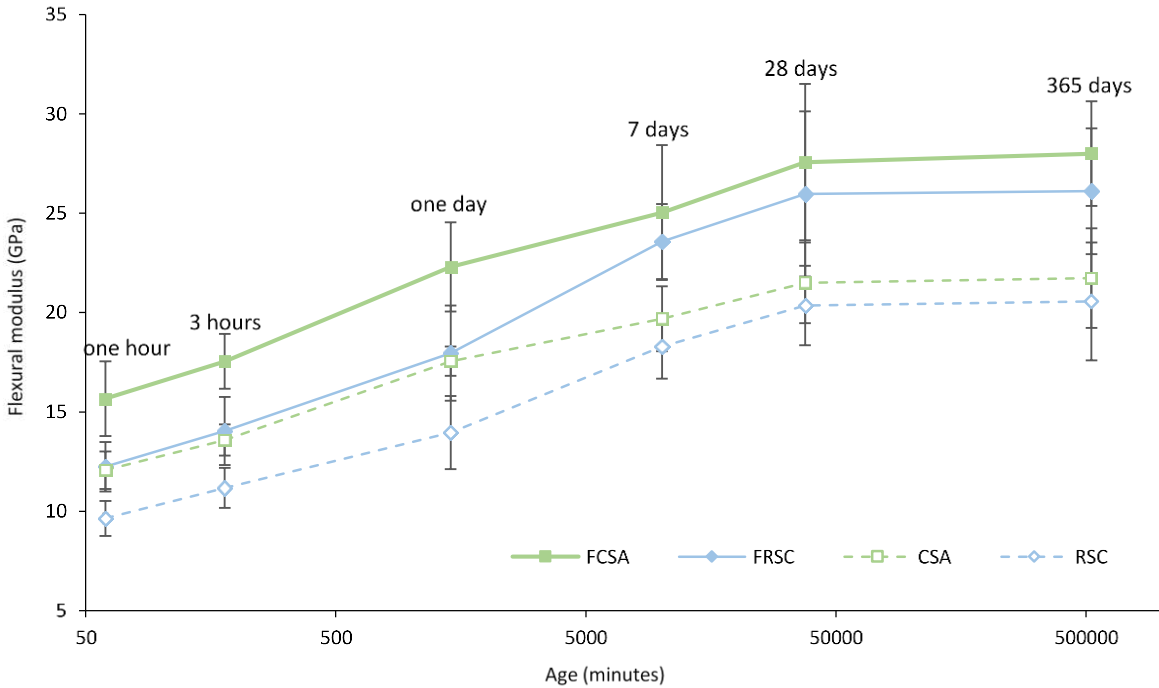


244  
245 **Figure 7.** Load-deflection response of rapid hardening fibre reinforced mortars tested at different ages: (a) FCSA;  
246 (b) FRSC

247 **3.2.3. Flexural modulus of elasticity ( $E_{fm}$ )**

248 The flexural modulus of elasticity ( $E_{fm}$ ) was determined from load-deflection curves using elastic analysis  
249 and ignoring shear deformations.  $E_{fm}$  is the maximum flexural modulus between 30 – 60% of the peak load  
250 ( $P_{peak}$ ) [37]. Figure 8 shows the development of  $E_{fm}$  and related standard deviations over time for all mixes.  
251 The plain mortar mixes are shown in dotted lines. As with flexural strength, the stiffness of the mixes  
252 develops quickly and reaches around 90% of the one year modulus within 7 days.

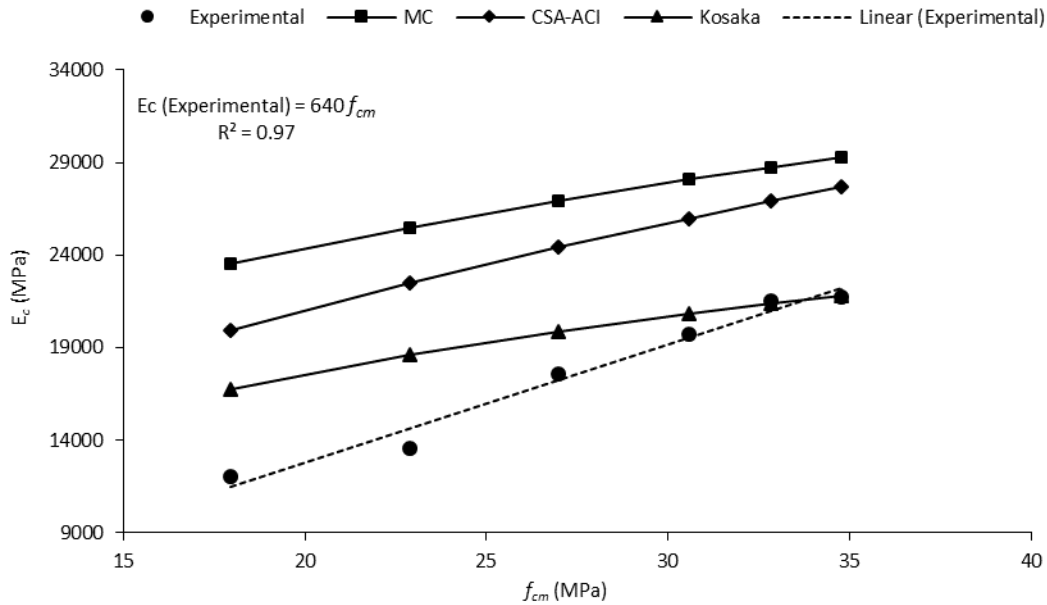
253 The fibres have a remarkable effect on the modulus of elasticity. FCSA and FRSC have higher  $E_{fm}$  compared  
 254 to CSA and RSC mixes respectively with the highest noticeable increase (29.7%) for FCSA occurring at one-  
 255 hour of age. This behaviour was not reported in [33] and [38] who only noticed a marginal effect on the  
 256 modulus of concrete with fibre addition. The remarkable increase in modulus of elasticity, though also  
 257 reflected in the flexural strength, is beyond what is expected from a perfect composite. This may be  
 258 partially due to fibre alignment, but also to the slightly longer mixing time that was necessary to integrate  
 259 the fibres. An increase of approximately 36% in the modulus of elasticity of OPC based mortars reinforced  
 260 with 2% (by volume) industrial steel fibres was reported in literature [39].



261  
 262 **Figure 8.** Flexural modulus ( $E_{fm}$ ) of fast setting fibre reinforced mortars as a function of time  
 263 To estimate the modulus of elasticity of the mixes, based on compressive strength, equations from Model  
 264 code [17], ACI 318-05 [40] and Kosaka et al. [41] were used. The latter equation was developed specifically  
 265 for mortars. The estimated modulus of elasticity ( $E_c$ ) for CSA (using the above equations) is presented in  
 266 Figure 9. As shown, the equations overestimate  $E_c$  for CSA mix, especially at the early ages. It should be



267 noted that both Model code and ACI code adopt equations that use the 1/3 and 1/2 power of  $f_{cm}$   
 268 respectively. However, the results show that for these mortars, the linear relationship is more appropriate  
 269 and the constant values of 720, 580, 640 and 520 were determined by regression analysis for FCSA, FRSC,  
 270 CSA and RSC mixes respectively.



271

272 **Figure 9.** The relationship between  $f_{cm}$  and  $E_c$  using different equations for CSA mix

273 **3.2.4. Relationship between measured deflection and CMOD values**

274 A linear relationship between CMOD and average deflection is suggested in BS EN 14651:2005 [35], as  
 275 given below,

276 Average deflection (mm) =  $k \times \text{CMOD (mm)} + 0.04 \text{ mm}$ ,  $k = 0.85$

277 This linearity has also been confirmed for FCSA and FRSC at all ages tested with coefficients of  
 278 determination  $R^2 > 0.99$ , but as expected with lower K values, between 0.55 and 0.65, due to the different  
 279 geometry of the testing arrangement. It should be noted that the CMOD measured by the clip gauge is  
 280 corrected for the position of the clip gauge using the BS EN 14651:2005 [35].

281 A relationship between deflection and CMOD can facilitate the testing of such materials by using clip  
282 gauges only to measure the CMOD as accurate measurement of deflection requires the use of a special  
283 frame (yoke) to obtain net deflection. It also provides a benchmark for comparisons.

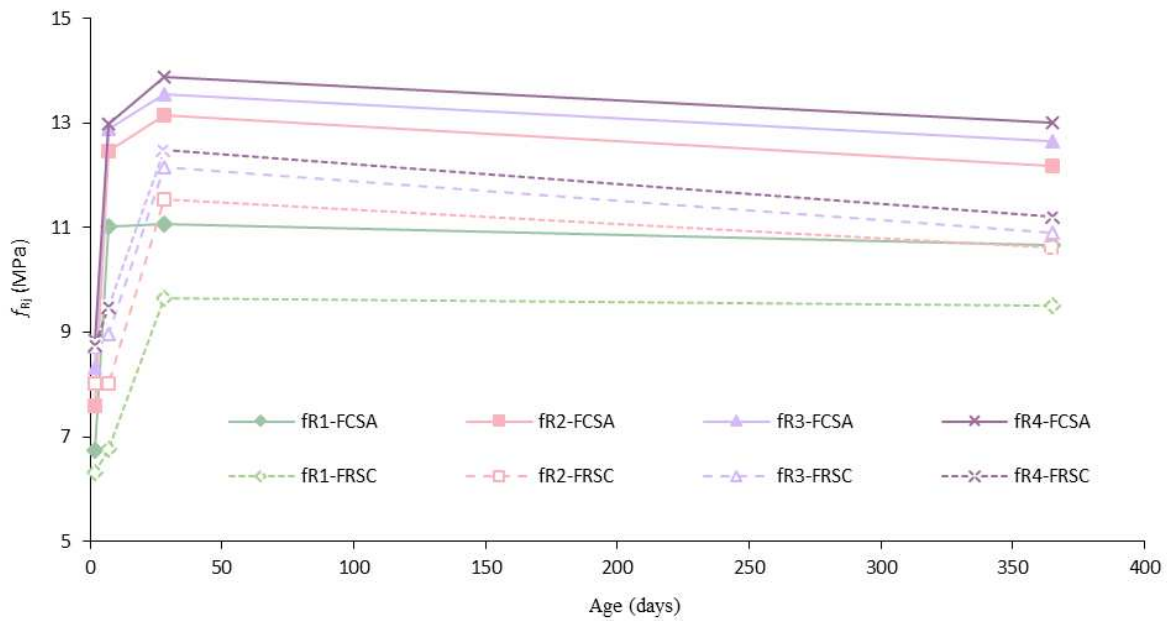
### 284 **3.2.5. Residual flexural tensile strength ( $f_R$ )**

285 RILEM TC 162-TDF [42] presents a methodology to calculate the residual flexural tensile strength of SFRC  
286 prisms, which was later adopted by BS EN 14651:2005 [33]. Residual flexural stresses ( $f_{R1}$ ,  $f_{R2}$ ,  $f_{R3}$  and  $f_{R4}$ )  
287 are calculated from the load-CMOD curves at 0.5, 1.5, 2.5 and 3.5 mm of CMOD, respectively. However,  
288 these CMODs are suggested for concrete prisms of 500 mm span length. For this study, the residual  
289 stresses are calculated at CMOD equal to 1/5 of those used for 500 mm span specimens; i.e. 0.1, 0.3, 0.5  
290 and 0.7.

291 Figure 10 shows the  $f_{Ri}$  values of all FCSA and FRSC mixes tested at different ages. The  $f_R$  values for FCSAs  
292 are shown in solid lines while FRSCs are shown in dashed lines. It is noticed that for both mixes the  $f_R$   
293 values continue to increase from CMOD 0.1 mm to 0.7 mm which shows the high efficiency of the RCSF in  
294 carrying the loads across cracks. This is also evidenced by the multiple cracks that form in some samples  
295 at, or more than, seven days of age. The residual strengths of FCSA are higher than those of FRSC for the  
296 same crack width, which implies better bond strength for RCSF in FCSA matrices.

297 The  $f_R$  values continue to increase with time for both FRC mixes and reach their peak values at 28 days.  
298 However, there is a slight strength reduction at one year compared to 28 days. This could be attributed  
299 to the effect of the conversion reaction occurring in the RSC cement. This is unlikely, however, as there  
300 was no reduction in compression strength at one-year of age. Another possible explanation is the effect  
301 of shrinkage on the bond strength of RCSF. This reduction in  $f_R$  is more obvious at higher CMOD levels (for  
302  $f_{R2}$  to  $f_{R4}$ ), which means that the frictional resistance along the fibres reduces slightly at one year.

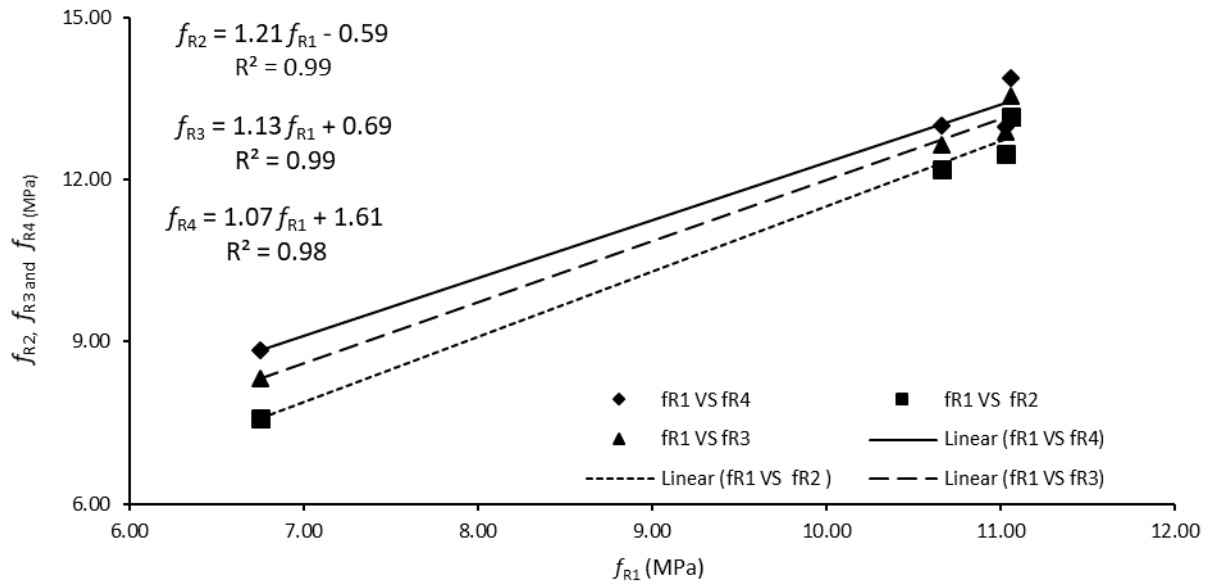
303 Figure 11 and Figure 12 show the relationship of  $f_{R1}$  vs  $f_{R2}$ ,  $f_{R1}$  vs  $f_{R3}$  and  $f_{R1}$  vs  $f_{R4}$  for FCSA and FRSC,  
 304 respectively. The values of  $f_{R2}$ ,  $f_{R3}$  and  $f_{R4}$  correlate very well with  $f_{R1}$  for FCSA prisms with  $R^2 \geq 0.98$ . A  
 305 similar trend was also found for FRSC prisms, however, with a relatively smaller coefficient of  
 306 determination ( $R^2 \geq 0.92$ ). A linear relationship between  $f_{R1}$  vs  $f_{R3}$ ,  $f_{R1}$  vs  $f_{R4}$  were also reported by  
 307 Zamanzadeh et al. [43] for unclassified RTSF. The strong correlation between the  $f_R$  values can lead to  
 308 simpler design guidelines.



309

310

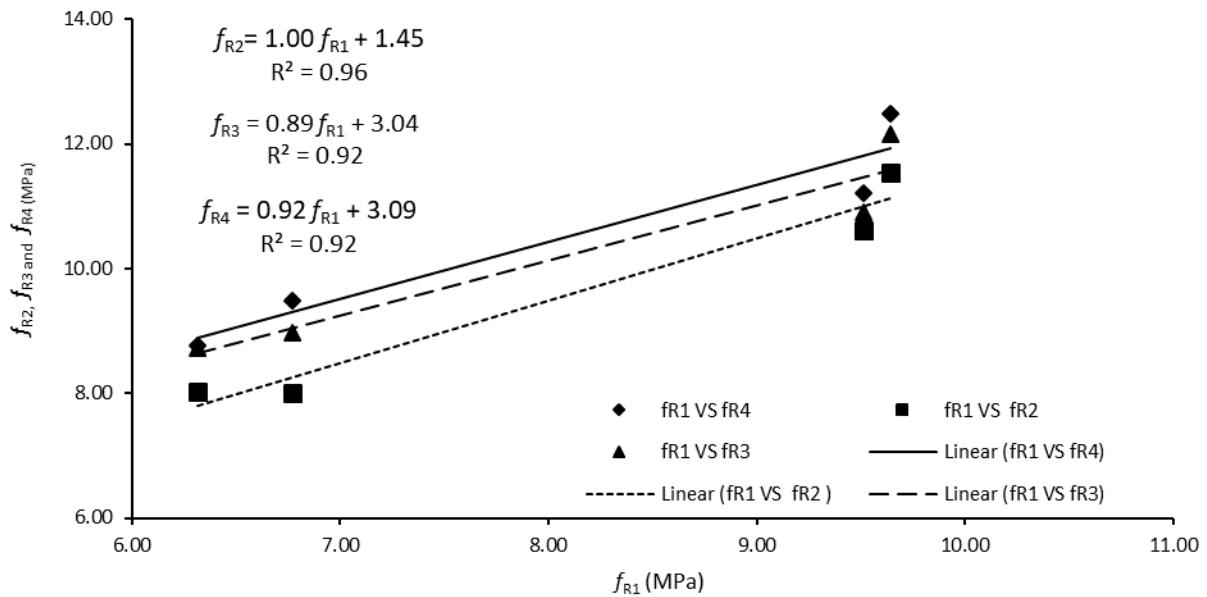
**Figure 10.**  $f_R$  values of FCSA and FRSC prisms (in MPa) development with age



311

312

**Figure 11.** Correlation between  $f_{R1}$  and  $f_{R2}$ ,  $f_{R1}$  and  $f_{R3}$ ,  $f_{R1}$  and  $f_{R4}$  of FCSA prisms



313

314

**Figure 12.** Correlation between  $f_{R1}$  and  $f_{R2}$ ,  $f_{R1}$  and  $f_{R3}$ ,  $f_{R1}$  and  $f_{R4}$  of FRSC prisms

315 **4. Numerical study**

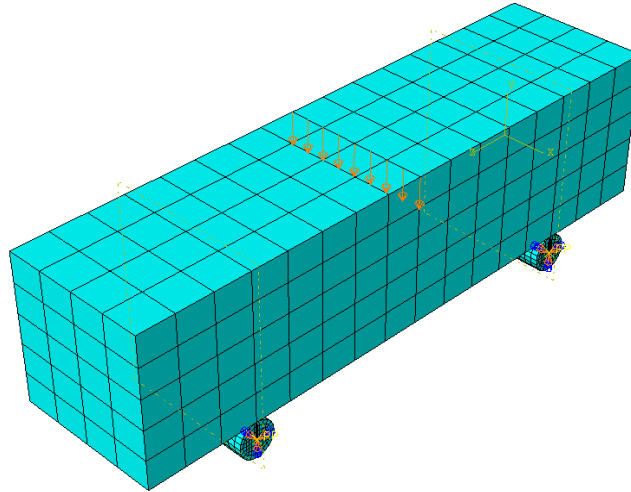
316 **4.1. FE modelling**

317 To model the flexural performance of these materials, the FE package ABAQUS is used, which offers three

318 material models for concrete simulation; Concrete Smeared Cracking (CSC), Brittle Cracking (BC) and

319 Concrete Damaged Plasticity (CDP) [44]. It was found that, for this application, CSC is prone to numerical  
320 instabilities soon after crack development. Similar issues were also reported in [45] when modelling SFRC  
321 prisms using CSC. Although the BC model was applied successfully to model FRSC [46], it was considered  
322 unsuitable for the current study as it assumes that the concrete remains elastic in compression. Since, due  
323 to the high flexural strength of the mortars, in this study, the material is expected to become non-linear  
324 in compression. Therefore, the analysis was performed by using the concrete damage plasticity (CDP)  
325 model for which the user can define the tensile and compression behavior of concrete in as many steps  
326 as required. In CDP, the ratio of biaxial to uniaxial compressive strength ( $\sigma_{b0}/\sigma_{c0}$ ) and the ratio of the  
327 second stress invariant on tensile meridian to that on the compressive meridian ( $K_c$ ) characterise the  
328 failure surface of concrete. The dilation angle ( $\psi$ ) and flow potential eccentricity ( $\epsilon$ ) are used to define the  
329 flow rule [44].  $\sigma_{b0}/\sigma_{c0}$  was taken as 1.2 (slightly higher than the value usually assigned for plain concrete  
330 due to presence of fibres),  $K_c$  was 0.667,  $\psi$  was  $31^\circ$  and after a sensitivity analysis for  $\epsilon$ , the default value  
331 of 0.1 was adopted. The CDP model can be regularised by using viscoplasticity to assist in overcoming  
332 convergence issues, that occur in materials exhibiting softening behaviour in implicit analysis  
333 computations, by permitting the stress to be outside the yield surface. Since high values of viscosity ( $\mu$ )  
334 compared to characteristic time increment can compromise the results, a value of zero was adopted.

335 Unnotched beams under 3-point bending were modelled in Abaqus with the same dimensions as tested.  
336 The mesh was kept constant at 10 mm size (Figure 13) and a 3D 20-noded quadratic brick element with  
337 reduced integration (C3D20R) was chosen, as second-order elements are very effective in bending-  
338 dominated problems [44]. Uniform displacement control loading was applied to minimise convergence  
339 problems and to better simulate the experimental loading conditions.



340

341

**Figure 13.** Prism assembly in Abaqus

342

#### **4.2. Evaluation of tensile constitutive equations**

343

RILEM TC 162-TDF (RILEM) [17], MODEL CODE 2010 (MC) [18], Barros et al. (Barros) [19] and Hu et al. (Hu)

344

[20] procedures were selected to derive the tensile constitutive equations. Although MC allows the use

345

of stress-crack width relationship, RILEM, Barros and Hu models all use stress-strain relationships, and

346

since stress-crack width relationship also leads to mesh dependency in CDP, it was decided to the use

347

stress-strain approach in modelling, to be able to make a direct comparison between different models.

348

The derived tensile  $\sigma$ - $\epsilon$  relationships (see Table 3) using the aforementioned procedures were

349

implemented in Abaqus to determine the load-deflection response of FCSA and FRSC prisms (at 28 days).

350

MC requires the maximum value of crack width ( $w_u$ ) to calculate the stress at ultimate strain. The value

351

0.5 mm was used for the max crack width as it corresponds to  $CMOD_3$ .

352

The predicted numerical load-deflection curves are compared against the experimental results for FCSA

353

in Figure 14. It can be seen that all the approaches fail to model the full behaviour of the prisms and for

354

most of them the analysis does not converge beyond 0.6 mm (even after using high values of  $\mu$ ). At 0.2

355

mm deflection, RILEM, MC and Barros overestimate the loading capacity by 29.44%, 16.65% and 7.11%

356

while Hu underestimates the loading by 14.88% respectively. Barros's model, however, can capture the

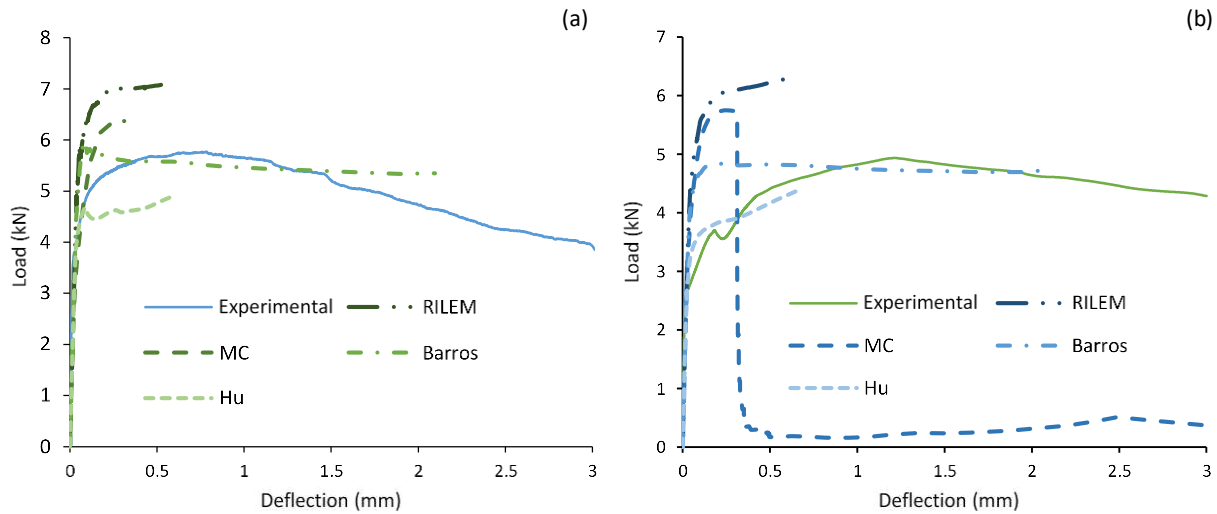
357 post-cracking behaviour of FCSA up to a certain extent. The models are even less effective in predicting  
 358 the flexural behaviour of FRSC (see Figure 14). Overall, none of the above models seem to be able to  
 359 capture the complete load-deflection behaviour of the tested specimens.

360 **Table 3**

361  $\sigma$ - $\epsilon$  relationships for FCSA and FRSC at 28 days using different approaches

Mixes	RILEM		MC		Barros		Hu	
	$\sigma$	$\epsilon$	$\sigma$	$\epsilon$	$\sigma$	$\epsilon$	$\sigma$	$\epsilon$
FCSA	9.473	0	2.980	0	7.037	0	4.771	0
	4.977	0.000263	3.311	0.000030	3.981	0.001056	2.986	0.001892
	5.140	0.024814	4.977	0.002319	3.751	0.103864	3.929	0.024857
	0.095	0.025000	4.561	0.012335	0.080	0.104000	0.050	0.025000
	0.090	0.500000	0.030	0.012500	0.074	0.500000	0.048	0.500000
		0.029	0.500000					
FRSC	6.165	0	3.354	0	4.580	0	3.105	0
	4.340	0.00017	3.727	0.000006	3.472	0.001066	2.604	0.002019
	4.619	0.024822	4.340	0.002333	3.370	0.103870	3.523	0.024864
	0.070	0.025000	4.145	0.012340	0.050	0.104000	0.040	0.025000
	0.065	0.500000	0.040	0.012600	0.046	0.500000	0.035	0.500000
		0.035	0.500000					

362



363

364 **Figure 14.** Comparison between experimental and numerical load-deflection curves at 28 days for: (a) FCSA; (b)

365

FRSC

### 366 4.3. Numerical approach using inverse analysis

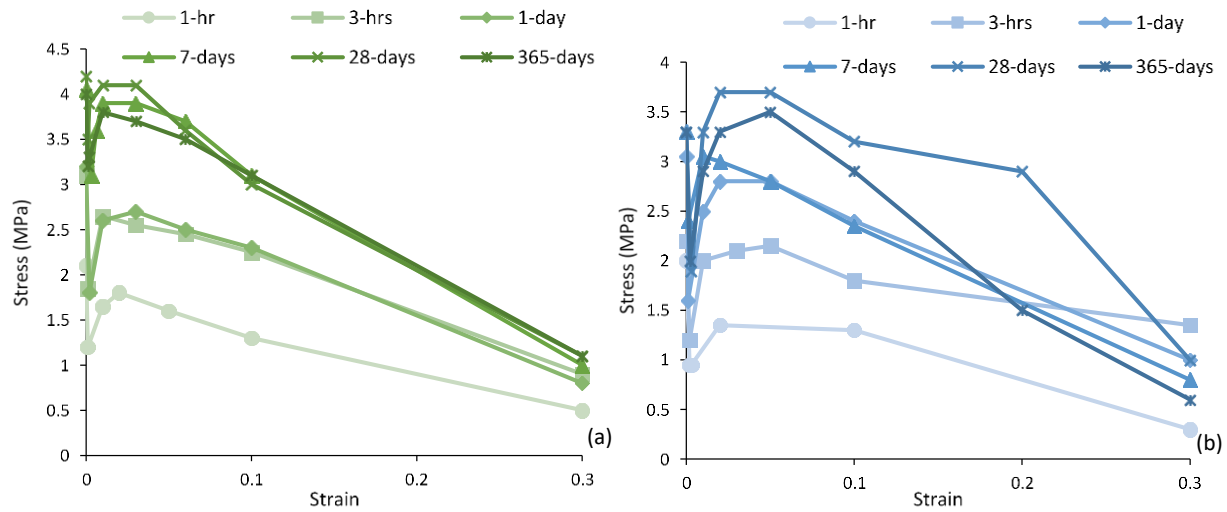
367 Inverse analysis was adopted to determine the post-cracking  $\sigma - \epsilon$  relationships for the different SFRC  
368 mixes and obtain a better prediction of the flexural performance of the tested specimens. The tensile  
369 properties are defined by using multilinear  $\sigma - \epsilon$  curves. The analysis is repeated while adjusting the tensile  
370 parameters until the numerical load-deflection curve matches the experimental response in capacity and  
371 energy dissipation within 2%.

372 The determined tensile  $\sigma - \epsilon$  curves shown in Figure 15 are then used to predict the structural behaviour  
373 of the FRC tested specimens. To better capture the flexural performance at larger displacements, the  
374 strain at failure should be accurately determined. The failure strain is calculated by dividing the ultimate  
375 width of crack (which is considered to be equal to half of the fibre length ( $l_f$ )) by the characteristic length.  
376 It was shown in a previous study on SFRC [45] that using a characteristic length of  $h_{sp}/2$  (the depth of a  
377 notched prism divided by 2) gives good results when converting displacements into equivalent strains.  
378 Thus, for this study, a value of 0.5 was adopted as a strain failure which is fairly close to  $l_f/2$  divided by  
379 half of the prism depth. It should be noted though that most tests were stopped at 5 mm deflection as  
380 not to damage the LVDTs and thus, complete failure was never reached. For design purposes, a max strain  
381 of 0.025 is deemed sufficient so as to prevent the development of large crack widths.

382 The predicted curves are shown together with the experimental results in Figure 16 through Figure 16. As  
383 expected, the predictions match well the results.

384 The results for FCSA at 28 days was further analysed (using the same material model for the 10mm mesh  
385 size) with two mesh sizes; 16.6 mm and 5 mm to examine the effect of mesh size. The results (Figure 17)  
386 confirm that there is a slight mesh dependence when using this approach.





387

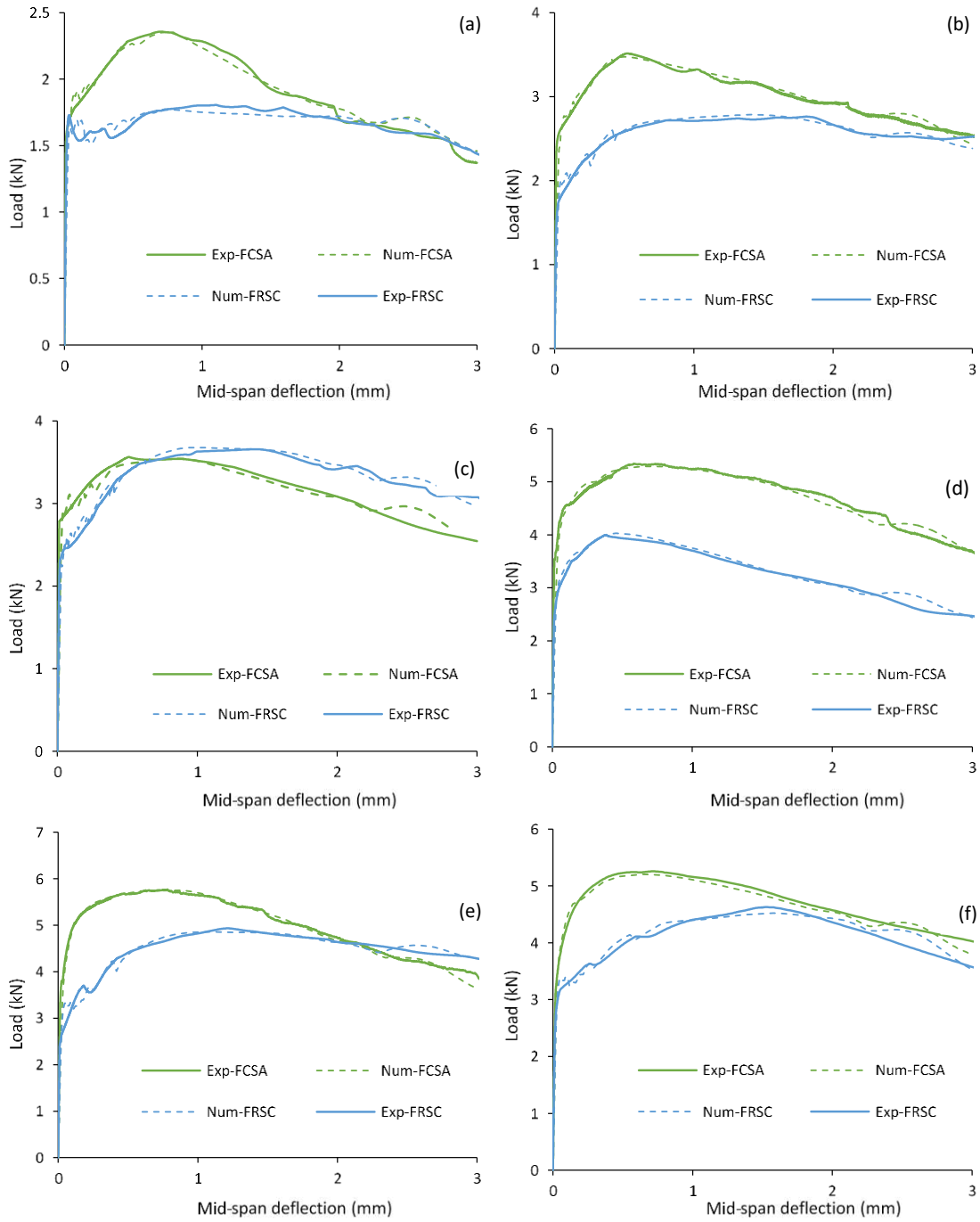
388

**Figure 15.** Tensile  $\sigma - \epsilon$  curves for mixes at different ages for: (a) FCSA; (b) FRSC

389 **4.4. Cracking**

390 In the CDP model, cracking can be assumed to initiate at points where the tensile equivalent plastic strain  
 391 is greater than zero and the maximum principal plastic strain is positive. The direction of the vector normal  
 392 to the crack plane is assumed to be parallel to the direction of the maximum principal plastic strain [44].  
 393 Figure 18 shows maximum principal strain contours for FCSA prism at 28 days. It is clear that the failure  
 394 of the prisms is characterised by tensile cracking at the midspan of the beam as occurred in the  
 395 experiments.

396 The crack width at the bottom of the specimens can be determined from the analysis by examining the  
 397 spreading of the beam using the horizontal deformation ( $U_3$ ) as shown in Figure 19. The crack width  
 398 determined at 3 mm of deflection are compared with CMOD values measured by the clip gauge in Table  
 399 4. The predicted values are slightly lower than the experimental values with the biggest error of 14.66%  
 400 (presented in brackets) for FCSA at 28 days. This confirms that the numerical models were not only  
 401 successful in predicting the flexural capacity, but also the crack widths of the tested prisms and as a result,  
 402 they could be used for further studies on repair layers.

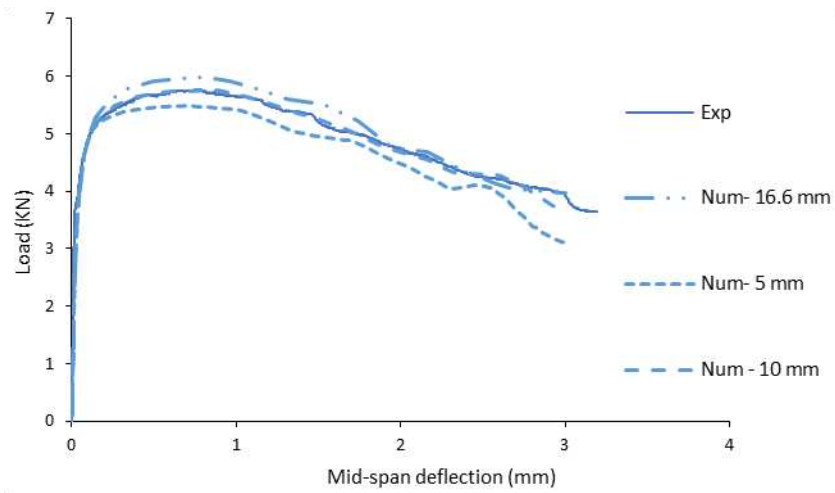


403

404 **Figure 16.** Experimental load-deflection versus numerical curves of FCSA and FRSC prisms at age of: (a) one-hour;

405

(b) three hours; (c) one-day; (d) seven days; (e) 28 days; (f) 365 days



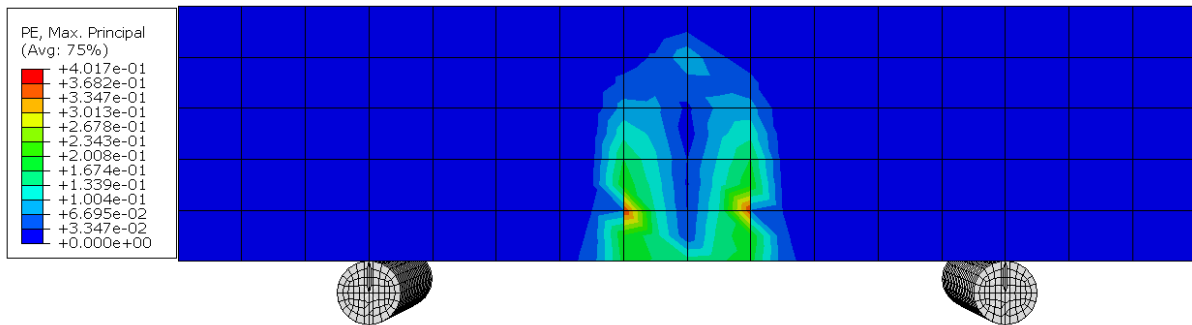
406

407

**Figure 17.** Experimental load-deflection curve of FCSA at 28 days versus numerical curves using three different

408

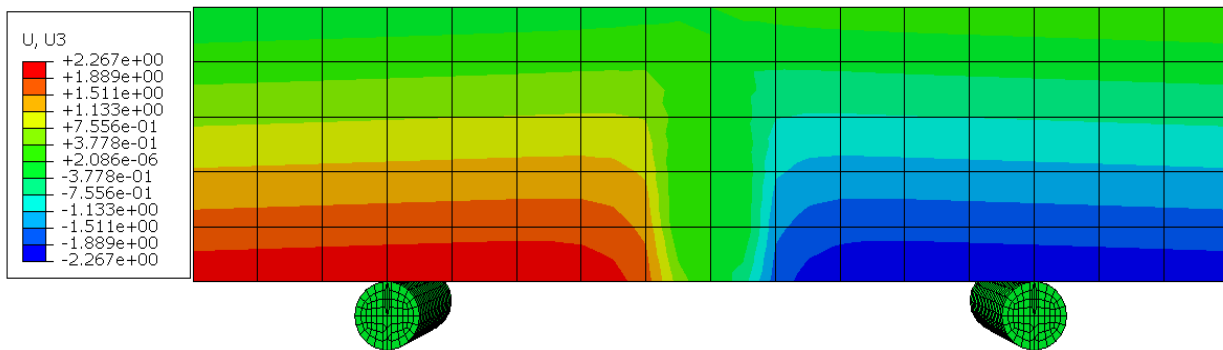
mesh sizes



409

410

**Figure 18.** Max principal strain contour for FCSA prisms at 28 days at the end of analysis



411

412

**Figure 19.** Horizontal displacement ( $U_3$ ) contour for FCSA prisms at 28 days at the end of analysis

413

414 **Table 4**

415 The measured and predicted crack widths for fibre reinforced mixes

Mix	Age	1hour	3 hours	1 day	7 days	28 days	365 days
FCSA	Numerical	4.68 (4.10)	4.64 (5.60)	4.68 (5.45)	4.52 (8.87)	4.54 (14.66)	4.64 (9.02)
	Experimental	4.88	4.903	4.953	4.96	5.32	5.10
FRSC	Numerical	4.37 (12.07)	4.60 (8.18)	4.59 (9.82)	4.71 (9.25)	4.57 (12.45)	4.6 (13.21)
	Experimental	4.97	5.01	5.09	5.19	5.22	5.3

416 Note: Values in brackets represent the error (%) between experimental and numerical crack width

417 **5. Conclusions**

418 Experimental and numerical investigations were performed on plain and fibre reinforced rapid hardening  
419 mortars. The main findings of this study are:

- 420 • Flexural strength evolves rapidly and both plain and fibre reinforced specimens achieved 90% of their  
421 one-year strength in one day. The specimens made with CSA cement showed higher flexural strength  
422 than those made with RSC cement tested at the same age due to the rigid dense crystal microstructure  
423 of the CSA cement.
- 424 • The fibres have a remarkable effect on the strength and modulus of elasticity of prisms. FCSA and  
425 FRSC mixes showed a flexural strength increase of approximately 36% to 70% and 24% to 41%  
426 respectively. For  $E_{fm}$ , an increase of 29.7% was found for FCSA at the age of one-hour. For compressive  
427 strength, the highest strength increase of around 24% was observed at one hour. No compressive  
428 strength reduction was noticed for any of the mixes tested in this study up to the age of one-year.
- 429 • The flexural residual strength for both FCSA and FRSC specimens continued to increase up to 0.7 mm,

- 430 which corresponds to  $CMOD_4$ . FCSA prisms show higher  $f_R$  than FRSC prisms for the same crack width.
- 431 The values of  $f_R$  continue to increase with time for both FRC mixes and reach their peak values at 28
- 432 days. However, there is a slight strength reduction at one year compared to 28 days.
- 433 • Strong correlations exist between  $f_{R1}$  and  $f_{R2}$ ,  $f_{R1}$  and  $f_{R3}$ ,  $f_{R1}$  and  $f_{R4}$  with  $R^2 \geq 0.98$  and  $R^2 \geq 0.92$  for
- 434 FCSA and FRSC, respectively.
- 435 • FE-predictions using CDP overestimate the loading capacity of FCSA and FRSC when using the tensile
- 436 constitutive laws based on RILEM TC 162-TDF, CEB FIB MODEL CODE 2010, Barros et al. Conversely,
- 437 the use of the models proposed by Hu et al. leads to underestimation.
- 438 • Inverse analysis was used successfully to obtain multilinear  $\sigma - \epsilon$  tensile curves and model the global
- 439 load-displacement behaviour.
- 440 • Numerical analyses using the refined  $\sigma - \epsilon$  curves were successful in capturing the cracking widths of
- 441 FRC tested prisms.

#### 442 **Acknowledgments**

443 The authors acknowledge the financial support of the Higher Committee for Education Development

444 in Iraq (HCED-Iraq) for the PhD studies of Hajir Al-musawi. The authors also thank Twincon Ltd for

445 material supply and in-kind contributions.

#### 446 **References**

- 447 [1] Winnefeld, F., Lothenbach, B., (2010). Hydration of calcium sulfoaluminate cements – experimental
- 448 findings and thermodynamic modeling. *Cem. Concr. Res.*, 40(8), 1239–1247.
- 449 [2] Ioannou, S., Paine, K., Quillin, K., (2010). Strength and durability of calcium sulfoaluminate based
- 450 concretes. In International Conference on Non-Conventional Materials and Technologies: Ecological
- 451 Materials and Technologies for Sustainable Building. University of Bath.

- 452 [3] Scrivener, K., (2003). Calcium Aluminate Cement. In J. Newman, *Advanced Concrete Technology*. 2/1-  
453 2/29. Oxford: ButterworthHeinemann.
- 454 [4] Campas, A., Scrivener, K. (1998). Calcium Aluminate Cements. In A. Campas, & K. Scrivener, *Lea's*  
455 *Chemistry of Cement and Concrete*, 709-771. Wobum: ButterworthHeinemann.
- 456 [5] Banthia, N., Gupta, R., (2009). Plastic shrinkage cracking in cementitious repairs and overlays. *Mater.*  
457 *Struct.*, 42(5), 567–579.
- 458 [6] Beushausen, H., Alexander, M.G., (2006). Failure mechanisms and tensile relaxation of bonded  
459 concrete overlays subjected to differential shrinkage. *Cem. Concr. Res.*, 36 (10), 1908-1914. Available at:  
460 <https://www.sciencedirect.com/science/article/pii/S0008884606001608>.
- 461 [7] Beushausen, H., Chilwesa, M., (2013). Assessment and prediction of drying shrinkage cracking in  
462 bonded mortar overlays. *Cem. Concr. Res.*, 53, 256–266. Available at:  
463 <http://dx.doi.org/10.1016/j.cemconres.2013.07.008>.
- 464 [8] Banthia, N., Zanotti, C. and Sappakittipakorn, M., (2014). Sustainable fibre reinforced concrete for  
465 repair applications. *Constr. Build. Mater.*, 67 (PART C), 405–412. Available at:  
466 <http://dx.doi.org/10.1016/j.conbuildmat.2013.12.073>.
- 467 [9] Jewell, R., (2015). Influence of Calcium Sulfoaluminate Cement on the Pullout Performance of  
468 Reinforcing Fibres: An Evaluation of the Micro-Mechanical Behavior. PhD Thesis. University of Kentucky.  
469 Available at: [http://uknowledge.uky.edu/ce\\_etds/27](http://uknowledge.uky.edu/ce_etds/27). [Accessed March 28, 2018].
- 470 [10] Swamy, R.N., Stavrides, H., (1979). Influence of fiber reinforcement on restrained shrinkage and  
471 cracking. In *Journal Proceedings. ACI J.*, 76(3), 443-460.

- 472 [11] Graeff, A.G., Pilakoutas, K., Neocleous, K., Peres, M.V.N.N., (2012). Fatigue resistance and cracking  
473 mechanism of concrete pavements reinforced with recycled steel fibres recovered from post-consumer  
474 tyres. *Eng. Struct.*, 45, 385–395. <https://doi.org/10.1016/j.engstruct.2012.06.030>.
- 475 [12] Pilakoutas, K., Guadagnini, M., (2013). Re-use of steel cord from tyres as reinforcement in sustainable  
476 construction – TSB Proposal. The University of Sheffield, Sheffield.
- 477 [13] Hu, H., Papastergiou, P., Angelakopoulos, H., Guadagnini, M., Pilakoutas, K., (2018). Mechanical  
478 properties of SFRC using blended recycled tyre steel cords and recycled tyre steel fibres, *Constr. Build.*  
479 *Mater.*, 187, 553-564.
- 480 [14] Frantzis, P., Baggott, R., (2000). Bond between reinforcing steel fibers and magnesium  
481 phosphate/calcium aluminate binders. *Cem. Concr. Compos.*, 22, 187–192.
- 482 [15] Frantzis, P., Baggott, R., (2003). Transition points in steel fiber pullout tests from magnesium  
483 phosphate and accelerated calcium aluminate binders. *Cem. Concr. Compos.*, 25, 11–17.
- 484 [16] Frantzis, P., (2006). Effect of Early-Age Temperature Rise on the Stability of Rapid-Hardening Cement  
485 Fibre Composites. *J. Mater. Civil Eng.*, 18, 568–575.
- 486 [17] RILEM TC 162-TDF, (2003).  $\sigma$ - $\varepsilon$ -design method, *Mater. Struct.*, 36(8), 560–567.  
487 <https://doi.org/10.1007/BF02480834>.
- 488 [18] F.I. du Béton, (2013). Fib Model Code for Concrete Structures 2010, Wilhelm Ernst &  
489 Sohn, Berlin, Germany.
- 490 [19] Barros, J.A.O., Cunha, V.M.C.F., Ribeiro, A.F., Antune J.A.B., (2005). PostCracking Behaviour of Steel  
491 Fibre-Reinforced Concrete. *Mater. Struct.*, 38, 47-56.
- 492 [20] Hu, H., Wang, Z., Figueiredo, F., Papastergiou, P., Guadagnini, M., Pilakoutas, K., (2018). Post-cracking

493 tensile behaviour of blended steel fibre reinforced concrete. *Struct. Concr.* Submitted for publication.

494 [21] Neocleous, K., Tlemat, H., Pilakoutas, K., (2006). Design issues for concrete reinforced  
495 with steel fibers, including fibers recovered from used tires. *J. Mater. Civ. Eng.*,  
496 18(5), 677–685. [https://doi.org/10.1061/\(ASCE\)0899-1561\(2006\)](https://doi.org/10.1061/(ASCE)0899-1561(2006)).

497 [22] Georjgin, J.F., Ambroise, J., Péra, J., Reynouard, J.M., (2008). Development of self-leveling screed  
498 based on calcium sulfoaluminate cement: Modelling of curling due to drying. *Cem. Concr. Compos.*, 30(9),  
499 769-778.

500 [23] ASTM C191, (2013). Standard Test Method for Time of Setting of  
501 Hydraulic Cement by Vicat Needle. *ASTM International*, (May), 1-8.

502 [24] RILEM, T.C., 119-TCE, (1997). Avoidance of thermal cracking in concrete at early ages. *Mater. Struct.*,  
503 30 (202), 451-464.

504 [25] BS EN 13892-2, (2002). Methods of test for screed materials — Part 2: Determination of flexural and  
505 compressive strength.

506 [26] JSCE-SF4, (1984). Standard for Flexural Strength and Flexural Toughness, Method of Tests for Steel  
507 Fiber Reinforced Concrete, Concrete library of JSCE, Japan Concrete Institute (JCI), Japan.

508 [27] Cost, T., (2008). Practical Semi-Adiabatic Calorimetry for Concrete Mixture Evaluation. In *TTCC/NCC*  
509 *Conference*.

510 [28] Aiello, M.A., Leuzzi, F., Centonze, G., Maffezzoli, A., (2009). Use of steel fibres recovered from waste  
511 tyres as reinforcement in concrete: pull-out behaviour, compressive and flexural strength, *Waste*  
512 *Manage.*, 29, 1960–1970. <https://doi.org/10.1016/j.wasman.2008.12.002>.

513 [29] Centonze, G., Leone, M., Aiello, M.A., (2012). Steel fibers from waste tires as reinforcement in



514 concrete: a mechanical characterization. *Constr. Build. Mater.*, 36, 46–57.  
515 <https://doi.org/10.1016/j.conbuildmat.2012.04.088>.

516 [30] Younis, K.H., Pilakoutas, K., (2013). Strength prediction model and methods for improving recycled  
517 aggregate concrete. *Constr. Build. Mater.*, 49, 688–701,  
518 <https://doi.org/10.1016/j.conbuildmat.2013.09.003>.

519 [31] Bjegovic, D., Baricevic, A., Lakusic, S., Damjanovic, D., Duvnjak, I., (2013). Positive interaction of  
520 industrial and recycled steel fibres in fibre reinforced concrete, *J. Civ. Eng. Manage.*, 19, S50–S60.  
521 <https://doi.org/10.3846/13923730.2013.802710>.

522 [32] Martinelli, E., Caggiano, A., Xargay, H., (2015). An experimental study on the postcracking behaviour  
523 of hybrid industrial/recycled steel fibre-reinforced concrete. *Constr. Build. Mater.*, 94, 290–298.  
524 <https://doi.org/10.1016/j.conbuildmat.2015.07.007>.

525 [33] Hu, H., Papastergiou, P., Angelakopoulos, H., Guadagnini, M. and Pilakoutas, K., (2018). Mechanical  
526 properties of SFRC using blended manufactured and recycled tyre steel fibres. *Constr. Build. Mater.*, 163,  
527 376-389. Available at: <https://www.sciencedirect.com/science/article/pii/S0950061817325230>.

528 [34] Herrmann, P., (2014). Investigation of fresh and hardened properties of Calcium sulfoaluminate (CSA)  
529 cement blends. *Mag. Civ. Eng.*, (3), 63-70. Available at:  
530 [http://www.engstroy.spb.ru/index\\_2014\\_03/07.pdf](http://www.engstroy.spb.ru/index_2014_03/07.pdf).

531 [35] BS EN 14651, (2005). Test method for metallic fibre concrete – Measuring the flexural tensile strength  
532 (limit of proportionality (LOP), residual). British Standards Institution, London, UK.

533 [36] Bordelon, A., (2011). *Flowable fibrous concrete for thin pavement inlays*. PhD Thesis. University of  
534 Illinois at Urbana-Champaign.

535 [37] Younis, K.H., (2014). *Restrained Shrinkage Behaviour of Concrete with Recycled Materials*. PhD Thesis.

536 University of Sheffield.

537 [38] Jafarifar, N., (2012). *Shrinkage behaviour of steel fibre reinforced concrete pavements*. PhD Thesis.

538 University of Sheffield.

539 [39] Dawood, E.T., Ramli, M., (2011). High strength characteristics of cement mortar reinforced with

540 hybrid fibres. *Constr. Build. Mater.*, 25 (5), 2240-2247.

541 [40] American Concrete Institute (ACI), (2011). Building code requirements for structural concrete and

542 commentary. (ACI 318M-11) Farmington Hills, MI.

543 [41] Kosaka, Y., Takeshi, T., Ota, F., (1975). Effect of coarse aggregate on fracture behavior of concrete

544 (part1). *J.A.C.*, 228, 1-11. Cited in Che, Y., (2010). *The development and behaviour of premix GRC suitable*

545 *for mass produced structural elements*. PhD Thesis, Department of Civil and Structural Engineering, The

546 University of Sheffield.

547 [42] RILEM. (2002). RILEM TC 162-TDF: Test and design methods for steel fibre reinforced concrete -

548 Bending test, final recommendation. *Mater. Struct.*, 35(253), 579–582.

549 [43] Zamanzadeh, Z., Lourenço, L. and Barros, J., (2015). Recycled steel fibre reinforced concrete failing

550 in bending and in shear. *Constr. Build. Mater.*, 85, 195–207. Available at:

551 <https://doi.org/10.1016/j.conbuildmat.2015.03.070>.

552 [44] ABAQUS 2017 Documentation, [Online].

553 [45] Tlemat, H., (2004). *Steel fibres from waste tyres to concrete; testing, modelling and design*. PhD

554 Thesis, Department of Civil and Structural Engineering, The University of Sheffield.

555 [46] Mohsin, S.M.S., (2012). *Behaviour of fibre-reinforced concrete structures under seismic loading*. PhD

556 Thesis. Imperial College London.